RSC Advances

Unexpected Production of Singlet Oxygen by Sub-Micron Cerium Oxide Particles and Enhanced Photocatalytic Activity against Methyl Orange

Journal:	*RSC Advances*
Manuscript ID:	RA-ART-03-2015-005208.R1
Article Type:	Paper
Date Submitted by the Author:	12-Jun-2015
Complete List of Authors:	C.R, Minitha; Bharathiar University, Physics Ramanathaswany, Pandian; IGCAR, Sankarakumar, Amirthapandian; IGCAR, Materials Science Group Ramasamy Thangavelu, Rajendra Kumar; Bharathiar University, Nanoscience and Technology

Journal Name

ARTICLE

Unexpected Production of Singlet Oxygen by Sub-Micron Cerium Oxide Particles and Enhanced Photocatalytic Activity against Methyl Orange

Dedicated to Prof.Dr.D.Mangalaraj, Dept. Of NanoScience and Technology, Bharathiar Univeristy, India on the occasion of his 60th Birthday

Received 00th January 20xx,
Accepted 00th January 20xx

DOI: 10.1039/x0xx00000x

www.rsc.org/

C.R. Minitha,[a] R. Pandian,[b] S. Amirthapandian[b] and R.T. Rajendra Kumar [a,c]

Abstract

Photodegradation of methyl orange (MO) by hydrothermally grown cerium oxide (CeO_2) particles has been investigated. It is observed that formation of oxygen vacancies and size of the particles increase with increasing growth temperature (230°C, 250°C, 270°C). Sample prepared at 270°C shows faster photocatalytic degradation of MO (~90%). Studies on reactive oxygen species generation reveal the unexpected production of singlet oxygen radicals along with super oxide anions. Further, singlet oxygen production found to increase with the growth temperature. A good correlation between size of the CeO_2 particles, singlet oxygen production and degradation of MO has been found. The production of singlet oxygen may be due to the synergy of oxygen vacancies and size of CeO_2 particles which enhance the charge accumulation at the surface of CeO_2 particles and thus increasing the band bending.

1. Introduction

Recently, water resources are getting polluted by textile industries which release various kinds of organic compound contaminated wastewater into the water reservoir without proper purification. This may cause severe problems to the green environment. Until now, cost effective and efficient degradation of dye molecules in aqueous solution is a great challenge. Metal oxide nanoparticles play a vital role in degradation of toxic dyes. Metal oxides such as titanium dioxide (TiO_2), zinc oxide (ZnO), tin oxide (SnO_2), tungsten trioxide (WO_3) and iron oxide (Fe_2O_3) have been studied extensively for waste water treatment applications. Metal oxides are used to decompose water into hydroxyl radicals and oxygen species to mineralize organic pollutants in wastewater to harmless end products by redox reaction.[1-3]

Nanocrystalline cerium oxide (Ceria, CeO_2), is a rare earth oxide with a wide band gap of $E_g \sim 3.5$ eV when compared to other metal oxides like TiO_2, ZnO etc. It has very attractive properties which play vital roles in the wide range of applications.[4-6] CeO_2 has been investigated by tuning the band gap and by controlling the size and shape of nanoparticles to develop more efficient photocatalytic behaviour of effluent.[2,7] Few reports are available for degradation and removal of azo dye from toxic water using pure CeO_2 nanoparticles as photocatalyst.[8-10] Few researchers have focused on the degradation of azo dyes using CeO_2 nanoparticles by doping, controlling the morphology using surfactant, and using templates.[11-13]

It is believed that the main mechanism of photodegradation could be controlled by the amount of reactive oxygen species (ROS) (O_2•- superoxide anion, $^1O_2$ - singlet oxygen, •OH - hydroxyl radicals) generation by nanoparticles.[14-16] Photo generated charge carriers from reactive surface of the nanoparticles can produce O_2•-, $^1O_2$ and •OH which reacts with the dye molecules and degrades to harmless end products.[1,17] These ROS are causative for the photo degradation of dyes by metal oxide nanoparticles. There are reports that ZnO and TiO_2 nanoparticles can generate all ROS but CeO_2 nanoparticles can produce only one type of ROS ($^1O_2$).[14]

[a] Advanced Materials and Devices Laboratory (AMDL), Department of Physics, Bharathiar University, Coimbatore - 641 046, India
[b] Materials Physics Division, Indira Gandhi Center for Atomic Research, Kalpakkam, 603102, India.
[c] Department of Nanoscience and Technology, Bharathiar University, Coimbatore - 641 046, India
[d] Corresponding author: rtrkumar@buc.edu.in

In this work, we demonstrate synthesis of CeO_2 particles at elevated temperature by hydrothermal method leading to the enhancement in photocatalytic activity. Furthermore, production of reactive oxygen species (ROS) is investigated; our results show the first experimental evidence for singlet oxygen ($^1O_2$) production by CeO_2 particles and it is attributed to the band bending induced by accumulation of charges near the surface. It is shown that proper control of surface oxygen defects and size of the nanoparticles may cause the production of more ROS which offers an opening to better insight about relationship between the band structure of nanoparticle and the photo degradation process. The combination of superoxide and singlet oxygen production by tuning the oxygen defects makes CeO_2 one of the suitable catalysts for the faster degradation of methyl orange.

2. Experimental

2.1 Preparation of submicron sized CeO_2 particles

CeO_2 nanoparticles are prepared by hydrothermal method. Cerium nitrate hexahytrate [$Ce(NO_3)_3.6H_2O$] and trisodium phosphate dodecahydrate [$Na_3PO_4.12H_2O$] (1:0.25M) are dissolved in 100ml of double distilled water and stirred well for about 10 minutes separately. Then 20ml of trisodium phosphate solution is added gradually to 60ml of cerium nitrate solution. The dispersed solution is transferred to the Teflon beaker of 100ml capacity and heated at different temperatures (230 ^oC, 250 ^oC, 270 ^oC) for 9 hours. Then the precipitates are collected and centrifuged several times with distilled water and ethanol. The final product is collected and dried in air at 60^oC overnight.[18] The CeO_2 particles grown at different growth temperatures of 230^oC, 250^oC and 270^oC are indicated as C1, C2 and C3 respectively in the manuscript.

2.2 Photo catalytic degradation and ROS Studies

Photocatalytic degradation activity of CeO_2 samples for methyl orange is studied under UV light irradiation. In this experiment 15 mg of sample is added into 15 ml of 15 ppm aqueous dye solution. The suspension is stirred for 5-10 minutes and kept under UV irradiation. A 20W - UV lamp of wavelength 364 nm is used as a source. The supernatant solution is collected at every 1 hour time interval and the change in intensity of absorption peak of dye is monitored using UV - Vis absorption measurement. The adsorption experiment is carried out in dark for initial adsorption property of CeO_2 particles towards dye for four hours. The supernatant solution is collected at 15 min and every 1 hour time interval and the change in intensity of absorption peak of dye is monitored using UV - Vis absorption measurement. Singlet oxygen and superoxide anion quantification were carried out by the procedure mentioned elsewhere[19]. For the detection of singlet oxygen ($^1O_2$) and super oxide anion (O_2•-), furfuryl alcohol (FFA, 0.85 mM) and nitroblue tetrazonium (NBT, 100 µM) respectively are used as the indicators. Chemicals are purchased from Sigma Aldrich. In our experiment, 15 mg of CeO_2 particles is added to 15 ml of ROS indicators. After different UV exposure time interval, suspension is collected and subjected to UV - VIS absorption analysis.[14]

2.3 Characterization of CeO_2 particles

The as-prepared samples are characterized using High Resolution Transmission Electron microscope (HRTEM) and Scanning Electron Microscope (SEM) are recorded on Zeiss Libra 200 and Zeiss SUPRA 55 respectively. Powder X- ray diffraction (XRD) is recorded with Bruker Advanced D8 with Cu Kα radiation (λ = 1.54Å) and it is used for studying its crystallinity, UV-Vis absorption spectra is obtained using Jasco V650 spectrophotometer for degradation and ROS studies and Raman spectroscopy is carried out at room temperature in a Horiba-Jobin, LabRAM HR system, using the 514 nm line of an Ar+ laser for excitation with optical lens of 50X magnification. BET surface area of the samples is measured on a Micromeritics pulse chemisorbs 2700 using nitrogen as adsorbate.

3. Results and Discussion

Fig. 1(a,b,c) shows the HRTEM images of CeO_2 particles C1, C2 and C3 respectively. The CeO_2 particles synthesized at 230^oC contain octahedron shaped particles (100 to 350 nm in size) along with more number of rods. It can be seen that on varying the growth temperature to 250^oC, size of the octahedron morphology became increased (100 to 500 nm in size). As the growth temperature further increases to 270^oC, morphology of the CeO_2 particles changes from octahedron to sphere (400 to 800 nm in size). The nanorod structures are extensively present in all morphologies which decrease in numbers with increase in growth temperature. The sizes of the particles are in sub-micron range with increase in growth temperature.

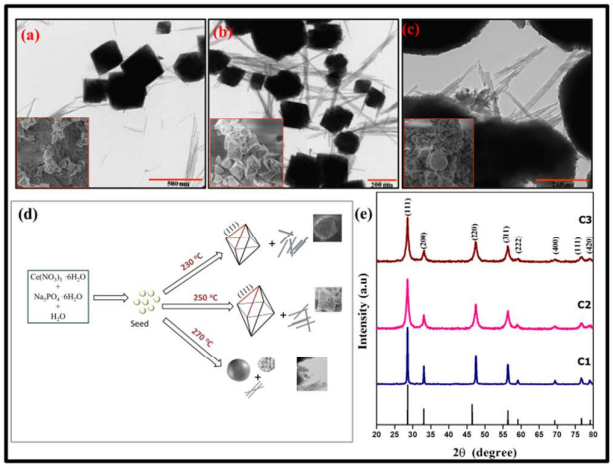

FIG. 1. HRTEM images of CeO_2 particles at different growth temperatures (a) 230^oC, (b) 250^oC, (c) 270^oC; Inset: FESEM images at 200 nm scale bar. (d) Schematic illustration of formation of CeO_2 particles. (e) XRD pattern of CeO_2 particles (C1 - 230^oC, C2 - 250^oC, C3 - 270^oC).

The schematic of CeO_2 particles formation obtained during different growth temperature is shown in Fig. 1(d). By tuning the hydrothermal growth temperature, morphology is modified from octahedron to sphere. At 270 °C, spheres are not uniform in their size; the range extends from few nanometers to hundreds of nanometers. The XRD pattern of CeO_2 particles grown at different growth temperatures are shown in Fig. 1(e). The obtained diffraction patterns of as-prepared particles show good crystalline nature and high purity (JCPDS card number: 65-2975). The diffraction pattern of CeO_2 is dominated by (111) lattice plane of reflection at $2\theta = 28.5°$ which shows that CeO_2 particles have cubic (fluorite) structure.[20]

Fig. 2 (a) shows the diffuse reflectance spectra (DRS) of pure CeO_2 particles. The band gap is determined using Kubelka–Munk plot which is given by $F(R) = (1-R)^2/2R$ where R is the reflectance of the sample.[20] The graph plotted for $[F(R)hv]^{1/2}$ vs photon energy, shows the direct band gap value of CeO_2 particles. The band gap value decreases (3.15 eV, 3.10 eV and 2.9 eV) as growth temperature increases. Red shift in band gap is observed in sample C3 when compared to C1 and C2. Patsalas et al.,[21] suggested that the red shift in band gap is due to increase in oxygen vacancies and the band gap decreases with the increase in oxygen vacancy level within the band gap. The decrease in band gap of sample C3 is due to the presence of additional phase of $CePO_4$.[22]

Fig. 2 (b) shows Raman spectra of precipitate obtained just after the mixture of the $Ce(NO_3)_3$ and Na_3PO_4 shows four bands at 471 cm^{-1}, 971 cm^{-1}, 1002 cm^{-1} and 1050 cm^{-1}. The vibration at 471 cm^{-1} are corresponds to symmetric deformation modes of the PO_4 groups and 971 cm^{-1} band is attributed to symmetric stretching of PO_4. The band around 1002 cm^{-1} is attributed to the symmetric stretching of PO_3 terminal groups from pyrophosphate. The bands at 1050 cm^{-1} come from the symmetric stretching vibrations of the PO_3.[23] The Raman spectra of C1 and C2 show band at 462 cm^{-1}, which assigned to dioxides with a fluorite structure.

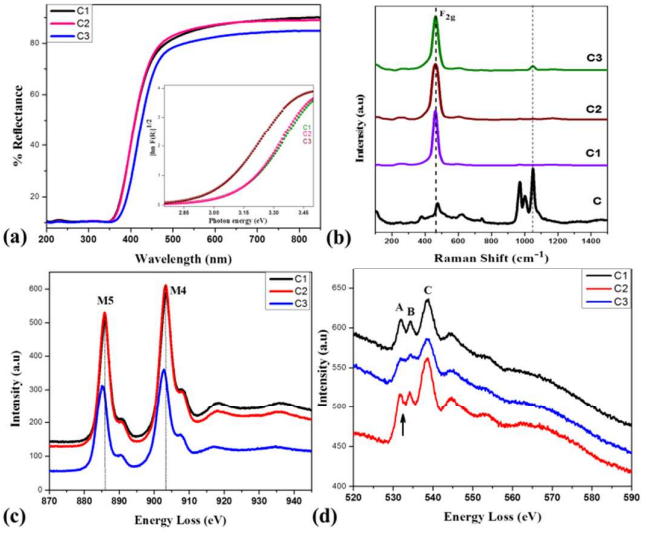

FIG.2. (a) Diffused reflectance spectra (DRS) of CeO_2 particles (Inset showing corresponding Kubelka - Munk plot, band gap determination by plotting [F(R)hv]1/2 Vs photon energy). (b) Raman Spectra of CeO_2 particles. EELS spectra of CeO_2 particles (c) Ce M4,5 edges of C1, C2, C3 & (d) O - K edges of CeO_2 (C1, C2, C3).

It has only one allowed Raman mode, which has F_{2g} symmetry and can be viewed as a symmetric breathing mode of the O atoms around each Ce.[24] In sample C3 show two bands at 462 cm^{-1} and very low vibration of 1048 cm^{-1}. It reveals that in sample C3 consists of CeO_2 and PO_3 vibration. The decrease in band gap of UV matches with the Raman spectrum.

Fig. 2 (c&d) shows electron energy loss spectra (EELS) of M4, M5 edges and O-K edges of CeO_2 particles respectively. The M4, M5 edges reflects the transitions of electron from 3d core level to unoccupied states (f states).[25-27] In sample C3, M5 and M4 maxima shows lower energy shift which indicates the presence of high Ce^{3+} states (Fig. 2c). EELS shift to lower energy indicates that the particles with lower oxidation states (Ce^{3+}) increases which is the result of creation of oxygen vacancies.[28] This indicates that the lower energy shift in the sample C3 is rich in oxygen vacancies when compared to C1 and C2 samples. The O-K edges of CeO_2 structures have decreased in C3 sample as shown in Fig. 2 (d). The peaks at 531.91 eV, 534.3 eV and 538.7 eV represents transitions to unoccupied states $Ce4f^0$, Ce 5d, Ce 5d from O 1s level respectively.[29] The intensity of the peak at 531.9 eV and 534.3 eV decreased while increasing the growth temperature (indicated by arrow mark). The disappearance of Ce^{4f0} peak states that Ce^{4+} is reduced to Ce^{3+}.[30] It confirms that Ce^{3+} enriches in sample C3 which also means that oxygen vacancy enriches in sample C3. From UV and EELS analysis affirms the increases oxygen vacancies with growth temperature.

To understand the effect of the surface area and porosity on the photocatalytic performance, the nitrogen adsorption desorption isotherms of two samples have been carried out, as shown in Fig. S3. The BET surface areas of C1 and C3 are 11 and 23 m^2/g respectively. Thus, BET surface area of C3 is larger than C1; this indicates that C3 has higher surface area towards dye. This could be responsible for the increase in adsorption of MO molecules on the sample C3 at dark conditions. In general, photocatalytic activity increase with increase in surface area of the nanocatalyts as more surface area facilitates more interaction of dye solution to the catalyst surface. However, the present work focus on the production of singlet oxygen ($^1O_2$) and increase in the production of $^1O_2$ in sample C3 might be responsible for the enhanced photocatalytic degradation. Fig. 3b shows the adsorption experiment in dark and removal efficiency of CeO_2 on MO dye. It clearly reveals that CeO_2 particles C1, C2 and C3 showed 22%, 24% and 30% of adsorption from initial dye concentration respectively. Whereas the samples C1, C2 and C3 shown 57, 58 and 90 % of MO degradation under UV illumination. One cannot rule out the possibility of the dye get adsorbed to nanocatalyst surface; however in our case photocatalytic action may be key factor behind the dye degradation. Fig 3c&d shows the degradation mechanism and degradation rate of methyl orange dye and CeO_2 particles under UV light irradiation. The MO dye molecules adsorbed on the surface of the CeO_2 and it might be excited by UV light photons to produce singlet states. Electrons can easily inject to the excited state of dye from the 4f band of CeO_2. Furthermore, the electrons from the Ce 4f band and the holes excited from the valence band migrate to the oxide surface and react with chemisorbed O_2 and H_2O molecules to generate reactive oxygen species.[9] Production of these ROS discussed in details later. From the degradation spectra of MO, there is an intense absorption peak at 467 nm Fig. S1. This is attributed to the presence of chromophoric compound (-N=N-) in the MO structure.[2] The C3 sample degrades methyl orange dye faster than C1 and C2.

The degradation rate of MO dye is plotted for (C_t/C_o) vs irradiation time, where C_t is the concentration of MO at time t and C_o is the initial concentration of MO. The rate of reaction is calculated using pseudo-first-order equation $\ln(C_t/C_o) = kt$, where k is the rate constant.[9] The rate constant of CeO_2 sphere like particles is estimated from the slope of the plot of $\ln(C_t/C_o)$ versus t, which is 0.354 h^{-1}. Rate constant of octahedron structures C1 and C2 are 0.134 h^{-1} and 0.181 h^{-1} respectively. The degradation rate of sphere shaped CeO_2 particle is 90% which is higher than the octahedron structures. While other two particles showed only 57% and 58% of dye degradation.

The reason behind the enhancement of photodegradation is further investigated by studying ROS production in CeO_2 particles. The ROS experiment has been done under UV irradiation for 4 hours. The absorption peak at 270 nm and 259 nm indicates the generation of singlet oxygen and super oxide anion respectively Fig. S2.

The previous reports show that the size of CeO_2 particle synthesized by hydrothermal method in the growth temperature range 90 °C to 200 °C were around 10 to 200nm.[31,32] In our case, the particle sizes are in the range of 100 to 350 nm and increases around 500 to 800 nm on increasing the growth temperature.

The CeO_2 particles could then agglomerate and self-assemble to give well-defined octahedrons. It is found that there are many nanorods present along with octahedron structures. Isotropic growth of octahedron structure has high Ce supply than anisotropic growth of nanorod structure. With increase in temperature to 250°C CeO_2 nano-rods differ in size and as temperature increases to 270 °C presence of nanorods decreases and CeO_2 spheres like structures are formed. This may be due to the reason that at the end of the reaction at elevated temperature Ce supply is low. Although the morphology evolution process of CeO_2 structures has been discussed, the basic formation mechanism is not completely understood.

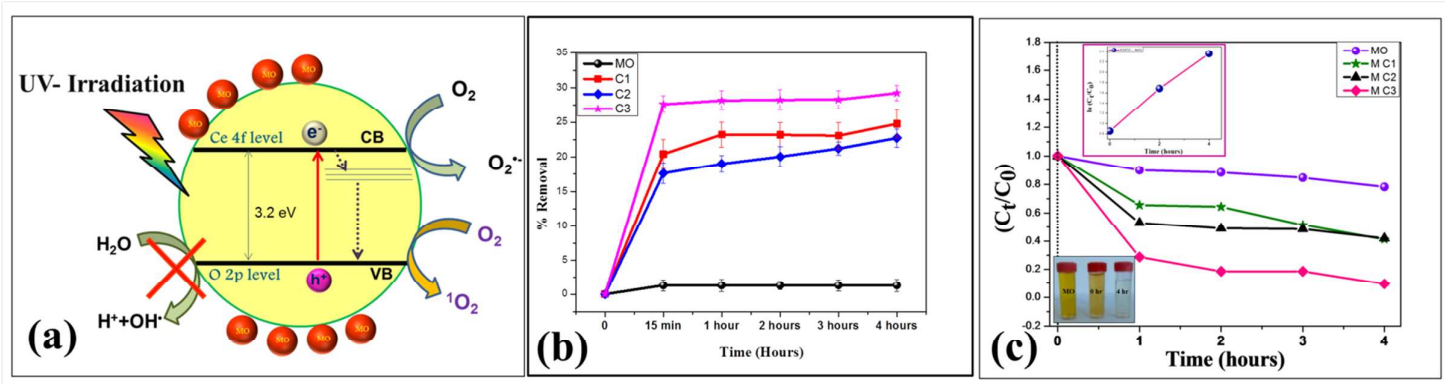

FIG.3. (a) Mechanism of photocatalytic degradation process. (b) Adsorption experiment in dark and Removal efficiency Vs Time. (c) Photocatalytic degradation rate of Methyl orange dye in the presence of CeO_2 particles grown at 230°C, 250°C and 270°C. (Insets: Photographic image of Pure, 0h and 4h of MO degradation and a plot of ln (C_t/C_o) vs irradiation time of sample C3).

Fig. 4 (a, b) shows the production of reactive oxygen species such as super oxide anion ($O_2^{\bullet-}$) and singlet oxygen ($^1O_2$). In this study, the average production of O_2•- is investigated (Fig. 4(a)) and it is found to be in the following order C1>C2>C3. The production of $O_2^{\bullet-}$ is already reported for CeO_2.[14] Interestingly, we could observe singlet oxygen production by CeO_2 particles (Fig. 4(b)). The average production of $^1O_2$ is high in the following order C3>C2>C1. It is interesting that all the samples produce singlet oxygen and the production of singlet oxygen increase with the growth temperature.

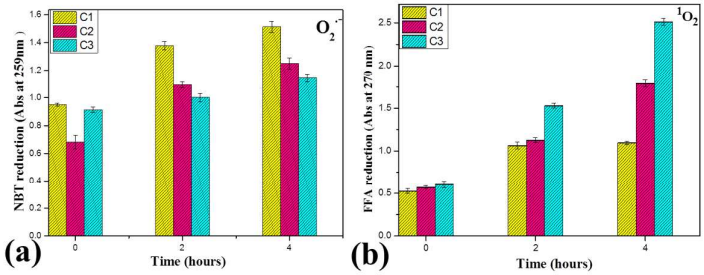

FIG. 4. (a) Bar graph for absorbance of NBT and FFA for the production of reactive oxygen species (a) $O_2^{\bullet-}$-Super oxide anion (b) $^1O_2$ - Singlet oxygen.

Further work has to be done for getting more insight about the growth mechanism and formation of ceria structures with different morphologies. There should be native oxygen vacancy defects present in all the samples. While growth temperature increases these oxygen vacancies are also increased. The red shift in UV spectra, Raman spectra and shift in EELS spectrum clearly reveals that the sample C3 has more oxygen vacancy states when compare to samples C1 and C2.

For ROS production, photocatalyst materials must have a conduction-band minimum more negative than the O_2/O_2•- level of water and a valence-band maximum must be more positive than the H_2O/O_2 level of water.[14] The nanoparticles like TiO_2 and ZnO produces all types of ROS because their band potential level favours all ROS production (Redox potential of ROS lies well within the band potential levels). Previous studies reported that CeO_2 particles are used as antioxidant and it could not produce sufficient ROS.[15] Yang Li et al, reported on the production of superoxide anion by CeO_2 nanoparticles of size about 25 nm that the band structure of CeO_2 can be favourable for the production of superoxide anion and not for singlet oxygen and hydroxyl radicals.[14] In our case, elevated hydrothermal growth temperature yielded relatively bigger size of CeO_2 particles (500 to 800 nm) with high oxygen vacancies and the exact mechanism of singlet oxygen production is unclear so far. Formation of space charge region on CeO_2 particle surface and associated surface band bending could alter the redox potential

of CeO_2 structures and may favour the singlet oxygen production. J. Liqiang et al.,[35] reported that the nanoparticles of smaller size have lesser charges on the surface and will not contribute to the band bending. When the size of the particle increases more charge accumulates to form space charge region and enhanced the surface band bending. In our case, the particle sizes are in the range of 100 to 350 nm and increases around 500 to 800 nm on increasing the growth temperature which is 10 to 30 times larger than the previous reports. In all the three samples native oxygen defects are observed and increases with the growth temperature. Therefore, the synergy of oxygen vacancies and CeO_2 particle size could facilitate more pronounced band bending in CeO_2 particles and production of singlet oxygen radicals. The rod like structures present in all samples (C1, C2 and C3) does not contribute to the band bending due to their smaller size.[35-37] Thus, sample C3 has higher degradation efficiency towards methyl orange due to the production of more ROS (singlet oxygen along with super oxide) as the result of enhanced band bending.

4. Conclusions

A good Correlation between CeO_2 particles size, singlet oxygen production and degradation of methyl orange has been found. The synergy effect of particle size and oxygen vacancies could induce band bending in CeO_2 particle that might generate $^1O_2$ radicals. The production of singlet oxygen along with superoxide could be responsible for the enhanced photocatalytic degradation performance. From our study, it is believed that the formation of more surface oxygen vacancies and increase in the particle size could tune the band positions of pure CeO_2 structures, and it also shows great promise to be used as a phototocatalyst.

Acknowledgements

C.R.M., and Dr. R.T.R thank Department of Science and Technology, Government of India for the financial support under SERB scheme (SR/FTP/PS-099/2011).

Notes and references

1 M. Dong, Q. Lin, H. Sun, D. Chen, T. Zhang, Q. Wu, and S. Li, *Cryst. Growth Des.,* 2011, **11**, 5002.
2 H. Li, G. Wang, F. Zhang, Y. Cai, Y. Wang and I. Djerdj, *RSC Adv.,* 2012, **2**, 12413.
3 D. Channei, B. Inceesugvorn, N. Wetchakun, S. Ukritnukun, A. Nattestad, J. Chen and S. Phanichphant, *Scientific reports.,* 2014, **4,** 5757.
4 H. Imagawa, A. Suda, K. Yamamura and S. Sun, *J. Phys. Chem. C.,* 2011, **115**, 1740.
5 W. Duan, A. Xie, Y. Shen, X. Wang, Y. Zhang and Jialin Li, *Ind.Eng.Chem.Res.,* 2011, **50**, 4441.
6 L. Zhong, J. Hu, A.Cao, Q. Liu, W. Song, and L. Wan, *Chem. Mater.,* 2007, **19**, 1648.
7 G.R. Li, D. Qu, L. Arurault, and Y. X. Tong, *J. Phys.Chem.C.,* 2009, **113**, 1235.
8 L. Qian, J. Zhu, W. Du, X. Qian, *Materials Chemistry and Physics.,* 2009, **115**, 835.
9 N.S. Arul, D. Mangalraj and T.W. Kim, *Appl. Phys. Lett.,* 2013, **102**, 223115.
10 P. Ji, J. Zhang, F. Chen and M. Anpo, *J. Phys. Chem. C.,* 2008, **112**, 17809.
11 M. K. Devaraju, S. Yin and T. Sato, *Crys.Eng.Comm.*, 2011, **13**, 741.
12 H. Yang, K. Zhang, R. Shi, and A. Tang, *J. Am. Ceram.Soc.,* 2007, **90**, 1370.
13 J. Saranya, K.S. Ranjith, P. Saravanan, D. Mangalaraj and R.T. Rajendra Kumar, *Materials Science in Semiconductor Processing.,* 2014, **26,** 218.
14 Y. Li, W. Zhang, J. Niu, and Y. Chen, *ACS Nano.,* 2012, **6**, 5164.
15 T. Xia, M. Kovochich, M.Liong, L.Madler, B. Gilbert, H. Shi, J. I. Yeh, J. I. Zink and A. E. Nel, *ACS Nano.,* 2008, **10,** 2121.
16 C. Y. Chen and C.T. Jafvert, *Environ. Sci.Technol.,* 2010, **44,** 6674.
17 Y. Liao, J. Brame, W. Que, Z. Xiu, H. Xie, Q. Li, M. Fabian and P.J. Alvarez, *Journal of Hazardous Materials.,* 2013, **260,** 434.
18 R. Yu, L. Yan, P. Zheng, J. Chen and X. Xing, *J.Phys.Chem.C.,* 2008, **112**, 19896.
19 K. Rajavel, R. Gomathi, S. Manian and R.T. Rajendralumar, *Langmuir.,* 2014, **30,** 592.
20 B. Choudhury and A. Choudhury, *Materials Chemistry and Physics.,* 2012, 131, 666.
21 P. Patsalas and S. Logothetidis, *Physical Review B.*, 2013, **68**, 035104; H. Chen, Y. Ni and X. Ma, *RSC Adv.,* 2014,**4**, 36553.
22 R. E. Rex, F. J. Knorr, and J. L. McHale, *J. Phys. Chem. C*., 2013, 117, 7949.
23 T. Masui, H. Hirai, N. Imanaka, and G. Adachi, *Phys. stat. sol. (a)*., 2008, **198**, 364.
24 V. D. Araujo, W. Avansi, H. B. de Carvalho,M. L. Moreira, E. Longo, C. Ribeirod and M. I. B. Bernardi, *CrystEngComm*, 2012, 14, 1150.
25 G. Strasser and F.P. Netzer, *J. Vac. Sci. Technol.A.,* 1984, **2**, 826.
26 L.Wu, H. J. Wiesmann, A. R. Moodenbaugh, R. F. Klie, Yimei Zhu, D. O. Welch, and M. Suenaga, *Phy.Rev. B.*, 2004, **69**, 125415.
27 T. Akita, M. Okumura, K. Tanaka, M. Kohyama, M. Haruta, *Catalysis Today.,* 2006, **117,** 62.
28 L.A.J. Garvie and P.R. Buseck, *Journal of Physics and Chemistry of Solids.,* 1999, **60**,1943.
29 D.R. Mullins, S.H. Overbury and D.R. Huntley, *Surface Science*., 1998, **409,** 307.
30 A.V. Soldatov, T.S. Ivanchenko, S.D. Longa, A.Kotani, Y.Iwamoto and A. Bianconi, *Phys.Rev. B.,* 1994, **50**, 5074.
31 T. Taniguchi, T. Watanabe, N.Sakamoto, N. Matsushita and M. Yoshimura, *Crystal Growth & Design.,* 2008, **8**, 3725.
32 Q.Yuan, H. H. Duan, L. Li, L.D. Sun, Y.W. Zhang and C.H. Yan, *Journal of Colloid and Interface Science.,* 2009, **335,** 151.
33 P.W. Voorhees, *J. Statistical Physics.,* 1985, **38**, 231.

34 L. Yan, R. Yu, J. Chen and X. Xing, *Crystal Growth & Design.,* 2008, **8**, 1474.
35 J. Liqiang, S. Xiaojun, S. Jing, C. Weimin, X. Zili, D. Yaoguo and F. Honggang, *Solar Energy Materials & Solar Cells.,* 2003, **79**,133.
36 A.W. Bott, *Current Separations.,* 1998, **17**, 87.
37 A. Hagfeldt and M. Gratzel, *Chem. Rev.,*1995 **95**, 49.